ACS Photonics

Article

pubs.acs.org/journal/apchd5

Enhancing the Sensitivity of Label-Free Silicon Photonic Biosensors through Increased Probe Molecule Density

Shuren Hu,[†] Yiliang Zhao,[‡] Kun Qin,[§] Scott T. Retterer,[∥] Ivan I. Kravchenko,[∥] and Sharon M. Weiss*[,†,‡,§]

[†]Department of Physics and Astronomy, Vanderbilt University, Nashville, Tennessee 37235, United States

[‡]Interdisciplinary Graduate Program in Materials Science, Vanderbilt University, Nashville, Tennessee 37235, United States

[§]Department of Electrical Engineering and Computer Science, Vanderbilt University, Nashville, Tennessee 37235, United States

[∥]Center for Nanophase Materials Sciences, Oak Ridge National Laboratory, Oak Ridge, Tennessee 37831, United States

Supporting Information

ABSTRACT: We report a greater than 5-fold increase in the detection sensitivity and a greater than 3-fold reduction in the response time of planar silicon photonic biosensors by increasing the density of probe molecules through the use of an in situ probe synthesis approach. DNA probe molecules are grown in a base-by-base manner with the desired sequence on silicon ring resonator and photonic crystal biosensors, resulting in a greater than 5-fold increase in surface area coverage compared to traditional covalent conjugation methods. With this approach, we demonstrate enhanced light−matter interaction, reduced optofluidic assay detection times, increased transduced signal sensitivity, and improved immunity toward false positives. This work highlights the importance of improving bioreceptor surface coverage densities in low mode volume photonic crystal devices and micrometer-scale ring resonators as a means of mitigating the effects of shrinking device sizes that otherwise limit the number of available target molecule capture sites and increase assay times.

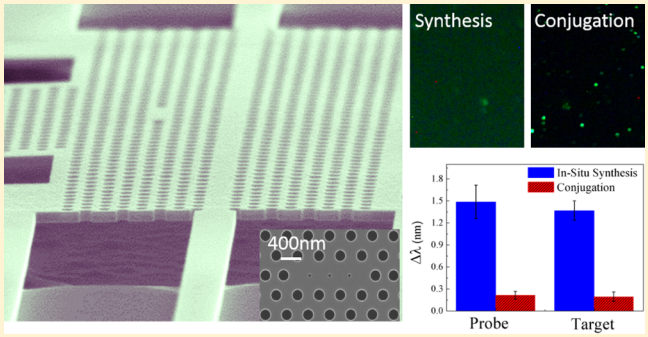

KEYWORDS: *biosensor, DNA, photonic crystal, ring resonator, label-free, silicon*

Point-of-care diagnostics are rapidly gaining increased traction within the research community and healthcare industry due to their potential for reducing healthcare costs, enabling personalized medications, and circumventing time-consuming laboratory tests.[1] Unlike conventional enzyme-linked immunosorbent assays, which indirectly test for the presence of target antigens or viruses through the use of secondary antibodies and time-dependent enzymatic reactions,[2] label-free biosensors directly transduce the presence of target molecules of interest into a measurable output signal and are therefore desirable for point-of-care diagnostics. Optical label-free biosensors based on silicon photonic structures, including ring resonators and photonic crystals, have the added advantage of utilizing complementary metal-oxide semiconductor (CMOS) compatible fabrication techniques for the production of high-volume, low-cost lab-on-a-chip sensors.[3−5]

Over the past decade, there has been rapid progress in the fabrication of low mode volume, nanoscale optical devices, such as microring resonators[6−10] and photonic crystals.[4,11−13] Strong localization of the optical field in such photonic resonators gives rise to enhanced light−matter interaction, which has enabled many advanced optoelectronic applications, such as low-energy ultrafast modulators and low-threshold lasers.[14−16] The strong light−matter interaction in these structures also results in a highly sensitive optical response to surface perturbations, which is ideal for surface sensing applications.[17] Moreover, light trapped within resonant cavities experiences longer interaction times with surface-bound molecules, further increasing the molecular detection sensitivity of resonant photonic structures and making silicon ring resonators and photonic crystals among the most promising biosensing platforms.

Microring resonators have been widely studied as label-free biosensors, including a recently commercialized optofluidic, multiplexed ring-resonator sensor.[5,18−20] Photonic crystals are believed to be the next generation in optical biosensors with performance metrics in detection sensitivity and detection time that could surpass those of ring resonators.[17,21−26] In photonic crystal cavities, photons are strongly confined by the photonic band gap within a subwavelength cavity region; photonic crystal resonators with ultrahigh quality factors, $Q > 10^6$, have been experimentally achieved.[11,13] Captured biomolecules of interest can therefore interact with a significantly higher field intensity in photonic crystals compared to ring resonators, which could significantly increase achievable detection sensitivities.[24] Moreover, the lower mode volume of most photonic crystals compared to ring resonators suggests that reduced analyte

Received: March 11, 2014
Published: June 20, 2014

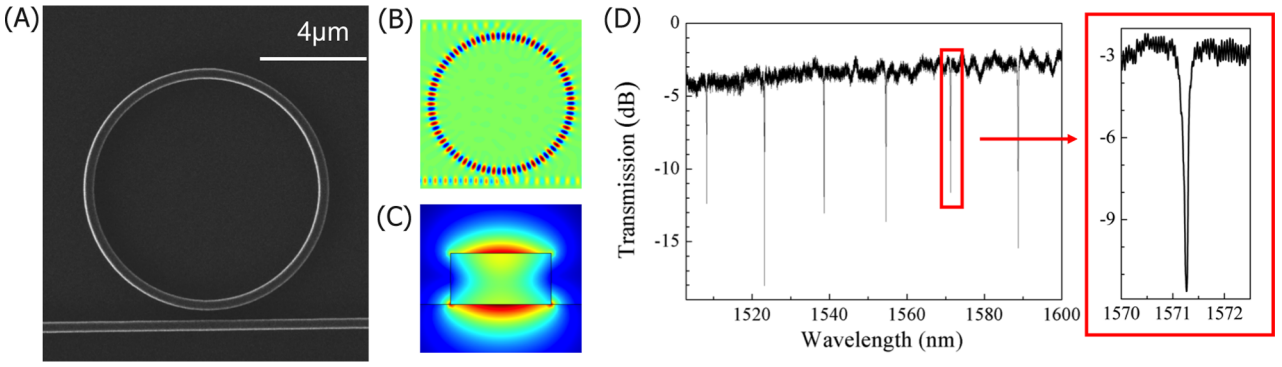

Figure 1. (a) SEM image of the 10 μm diameter ring resonator and 500 nm width waveguide. (b) On-resonance FDTD electric field distribution in the ring resonator and bus waveguide. (c) Cross-sectional field distribution for a TM mode waveguide. (d) Measured transmission spectrum of the 10 μm ring resonator with zoom-in on one resonance.

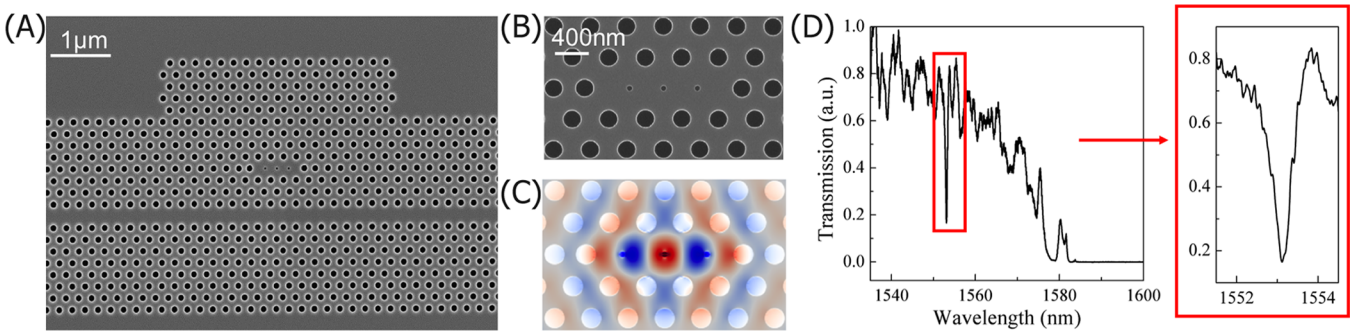

Figure 2. (a) SEM image of MHD photonic crystal device with a lattice hole radius of 100 nm and a lattice constant *a* of 410 nm. (b) Zoom-in SEM image of MHD cavity showing the defect holes, ~50 nm in diameter, and neighboring right and left lattice holes that are shifted 0.15*a* outward to achieve lower mode profile perturbation at the cavity edge. (c) Simulated electric field distribution (TE mode) for the MHD cavity showing strong field confinement in the defect hole region due to a slot waveguide-like effect. (d) Measured transmission spectrum of MHD photonic crystal with zoom-in on cavity resonance.

volumes and response times can be realized in photonic crystal sensors. Recently, Chen et al. reported a detection limit of 0.01 nM for cancer biomarkers, demonstrating great potential for ultra-low-concentration multiplexed assays.[24]

While the relatively small footprint of both microring resonators and photonic crystals is an advantage for achieving compact sensor devices, the reduced sensing surface area inherent to these devices limits the total number of capture sites for target molecules. Having a reduced number of capture sites poses two challenges. First, if not enough target molecules are captured on the sensor, a detectable signal cannot be transduced. Second, even if there are enough capture sites to enable a sensor transduction event, a detectable signal response for sub-nanomolar analyte concentrations may require increased sample volumes or assay times in order for target molecules to bind to a sufficient number of the probe capture sites. Additionally, these optical sensors will be more susceptible to false positives arising out of nonspecific binding events at the sensing surface. In order to achieve rapid, ultralow detection limits with microliter sample volumes, it is imperative to achieve a high surface density coverage of probe molecules that maximizes target capture with minimum incubation times. Without a sufficiently high probe molecule density, signal amplification, for example, through the use of a sandwich assay, must be implemented.[6] In this work, we report on in situ, base-by-base synthesis of single-stranded DNA (ssDNA) probe molecules directly onto silicon photonic sensor surfaces, resulting in over 5-fold increased ssDNA probe surface coverage and a more than 5-fold increased detection sensitivity compared to sensors functionalized with traditional ssDNA probe attachment methods. Importantly, in addition to the detection of complementary DNA sequences, ssDNA probes can also be used for detecting a variety of other types of molecules when the proper sequence and molecule conformation is designed (i.e., ssDNA aptamer probes[27,28]). The in situ probe synthesis approach opens up possibilities for rapid signal transduction of single biomolecule binding events by monitoring shifts of resonance wavelengths with analyte concentrations down to the femtomolar range with microliter sample volumes. The development of these optical label-free biosensors is therefore of great importance for the early clinical diagnosis of many life-threatening diseases.[26]

RESULTS AND DISCUSSION

Silicon Photonic Sensor Platforms. The two prototypical silicon photonic sensor platforms employed in this work, the microring resonator and the photonic crystal microcavity, are shown in Figures 1 and 2. Figure 1a shows a scanning electron microscope (SEM) image of a 5 μm radius microring resonator coupled to a 500 nm width waveguide. The gap between ring and waveguide is 300 nm, which meets the critical coupling condition and gives the highest extinction ratio by finite difference time domain simulations (FDTD). Figure 1b shows the electric field distribution of the *z*-normal plane calculated by FDTD simulations for TM-like polarization. The cross-section of the electric field distribution (Figure 1c) indicates that the

dx.doi.org/10.1021/ph500075g | ACS Photonics 2014, 1, 590−597

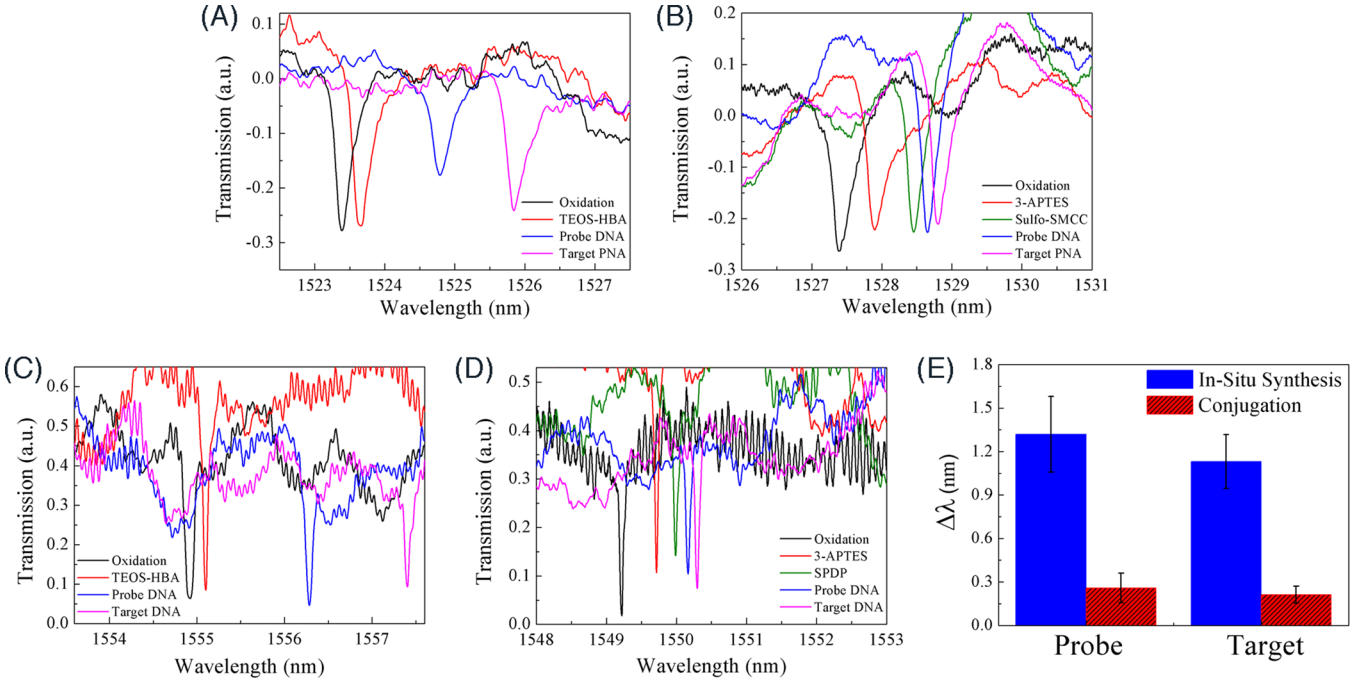

Figure 3. Transmission spectra of ring resonators functionalized by in situ synthesis of ssDNA probes (a, c) and direct conjugation of ssDNA probes (b, d). (a) and (b) show ssPNA target detection, while (c) and (d) show ssDNA target detection. Each spectrum corresponds to a transmission measurement made after a different molecule was attached to the surface (see Methods section for details). A significantly larger resonance shift upon both ssDNA probe attachment and ssPNA/ssDNA target hybridization results for the ring resonator prepared using the in situ probe synthesis approach. (e) Average resonance wavelength shifts for probe and target binding on four ring resonator sensors functionalized by the in situ ssDNA probe synthesis method and four ring resonators functionalized by the traditional ssDNA probe conjugation technique.

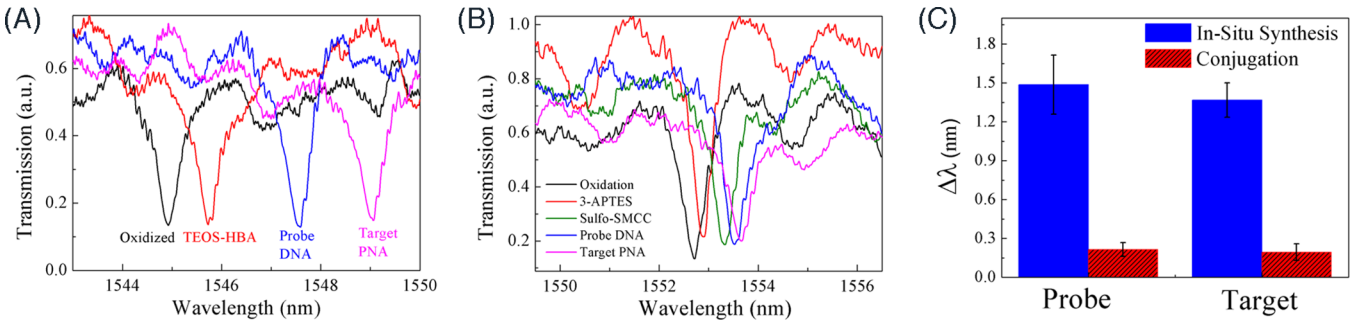

Figure 4. Transmission spectra of MHD photonic crystals functionalized using (a) in situ synthesis and (b) direct conjugation methods for probe molecule attachment. Each spectrum corresponds to a transmission measurement made after a different molecule was attached to the surface (see Methods section for details). The ssDNA probe attachment by in situ synthesis, as well as subsequent ssPNA hybridization, results in a significantly larger resonance wavelength shift compared to the direct conjugation method. (c) Average resonance wavelength shifts for probe and target binding on three MHD photonic crystals functionalized by the in situ ssDNA probe synthesis method and three MHD photonic crystals functionalized by the traditional ssDNA probe conjugation technique.

field is primarily localized on the top and bottom surfaces of the ring resonator, where molecules are most likely to be captured. TM ring resonators are known to be more sensitive to surface changes compared to TE-like microring resonators,[29] wherein the field is mainly distributed within the waveguide core. Figure 1d shows a typical transmission spectrum of the 5 μm radius ring resonator. The Q-factor is approximately 12 000, and the free spectral range is approximately 15.5 nm.

Figures 2a,b show SEM images of the 2D photonic crystal resonator used in this study. The multihole defect (MHD) design for an L3 cavity introduced by Kang et al. is employed to increase the total surface area for probe molecule capture and to enhance the electric field−analyte overlap through the slot waveguide-like effect that takes place inside the defect holes.[22,30] The MHD photonic crystal sensor used in this study has a defect hole diameter of approximately 50 nm and a center-to-center defect hole spacing of 380 nm, which was previously shown to achieve the maximum Q-factor for the structure.[30] With the MHD design, both traditional photonic crystal surface sensing, which relies on evanescent field interaction with surface-bound molecules, and sensing within the volume of the defect holes where the resonant mode is localized are utilized for detecting biomolecule capture. Figure 2c shows the simulated electric field distribution in the MHD cavity as calculated by FDTD analysis for TE-polarized light. Since the electric field is highly concentrated in the defect region, capture of biomolecules within the defect holes will strongly perturb the field distribution and result in large shifts in the resonance wavelengths. A typical transmission spectrum

dx.doi.org/10.1021/ph500075g | ACS Photonics 2014, 1, 590−597

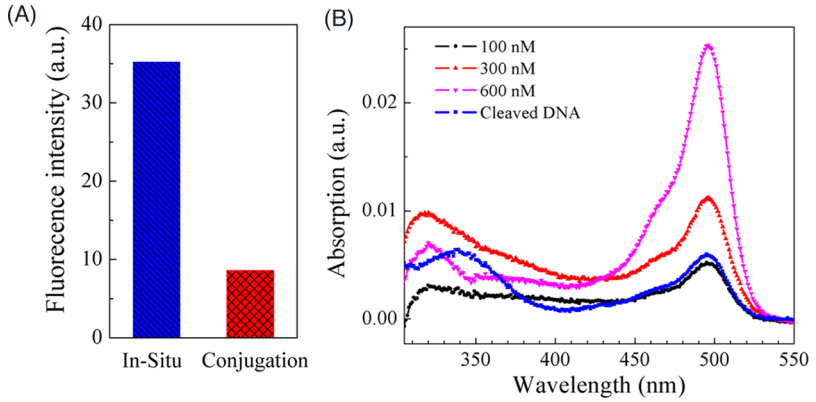

Figure 5. (A) Comparison of fluorescence intensity of silicon samples functionalized with in situ synthesized ssDNA probes and directly conjugated ssDNA probes that have been fluorescently tagged with FAM6 dye. Fluorescence images are shown in Figure S4-1. (B) Absorbance spectra of solutions with known concentrations of FAM6-labeled DNA (100, 300, 600 nM) and the solution containing molecules cleaved from the surface of a silicon sample functionalized with directly conjugated FAM6-labeled probe DNA molecules (cleaved DNA). The concentration of probe DNA conjugated to the silicon surface (~130 nM) is obtained through comparison to the intensity of the FAM6 absorption peak (495 nm).

with a resonance wavelength near 1550 nm and a *Q*-factor of ~4000 is shown in Figure 2d for the MHD L3 photonic crystal.

Sensitivity Enhancement with Increased Probe Molecule Surface Coverage. Two methods of surface functionalization were performed on the silicon microring resonators and photonic crystals, as described in the Methods section. For sensors functionalized by in situ probe synthesis using the phosphoramidite method in which single DNA bases are added in a stepwise fashion, a single silane molecule is sufficient to attach the probe molecules to the oxidized silicon surface. For sensors functionalized using a traditional conjugation technique in which the full sequence ssDNA probe molecules are directly attached to the sensor, a different silane molecule and a heterobifunctional cross-linker molecule are utilized to enable probe molecule attachment to the oxidized silicon surface. Both silanization approaches have been shown to lead to nearly complete surface coverage of the sensors by silane molecules, which are then available for additional molecule attachments.[31] It has been previously reported in the porous silicon material system that the density of directly conjugated ssDNA probe molecules is 30−40% lower than in situ synthesized ssDNA probe molecules inside nanoscale pores, in part due to steric hindrance between the negatively charged ssDNA molecules.[31] This result suggests that in situ synthesis may be advantageous for functionalizing planar silicon photonic biosensors.

Figure 3a,c and Figure 4a show the sensing results for the hybridization of ssDNA and single-strand peptide nucleic acid (ssPNA) target molecules to silicon microring resonators and photonic crystals, respectively, which have been functionalized by in situ synthesized ssDNA probe molecules. Figure 3b,d and Figure 4b show the sensing results for ssDNA and ssPNA hybridization to silicon microring resonators and photonic crystals, respectively, which have been functionalized by directly conjugated ssDNA probe molecules. The sensing experiments shown in Figure 3a,b were performed using 100 μM target ssPNA, while Figure 3c,d show the sensing results for 100 nM ssDNA detection. Experiments were also conducted using a variety of other target molecule concentrations (see Supporting Information S1), suggesting that the silicon photonic sensors respond similarly to ssPNA and ssDNA target molecules and that the probe molecule binding sites are nearly all saturated when exposed to at least a 100 nM concentration of complementary target molecules. Sensors functionalized with in situ synthesized ssDNA probe molecules were shown to detect 10 nM target ssDNA, while sensors functionalized with directly conjugated ssDNA probe molecules could detect 50 nM target ssDNA. It is anticipated that if only the active sensor regions of the silicon photonic chips were functionalized for target molecule detection to minimize target binding in regions where the mode is not confined, sensors functionalized with in situ synthesized probes would be capable of target ssDNA detection below 10 fM.

For both the ring resonators and photonic crystals, the resonance shifts after ssDNA probe and ssDNA/ssPNA target attachment are significantly larger when in situ synthesized ssDNA probe molecules are utilized. In all cases, when a sufficiently high concentration of target molecules was used to saturate the available probe molecule binding sites (i.e., > 100 nM), the resonance wavelength shift resulting from target molecule hybridization was nearly the same as the resonance shift following probe attachment. This suggests that nearly 100% hybridization efficiency can occur for all probe molecule densities employed in this work. Since the magnitude of the resonance shift is a direct indication of the number of molecules attached to the surface, we can infer that the enhanced sensitivity of the in situ probe-functionalized sensors is due to the increased number of probe molecules on the surface available for hybridization. The in situ synthesis method enables the increased probe coverage by adding uncharged DNA monomers in a base-by-base fashion (see Methods section for details), which reduces the effects of steric hindrance and charge repulsion that challenge the immobilization of longer, negatively charged ssDNA molecules. In an attempt to minimize charge repulsion in the conjugated probe ssDNA molecules, $MgCl_2$ was added, as described in Supporting Information S2; however, only a slight increase in the resonance wavelength shift corresponding to a small increase in the probe molecule coverage resulted even after an increased incubation time and increased probe molecule concentration were utilized.

As summarized in Figures 3e and 4c, the increased resonance shift due to probe molecule attachment and the detection sensitivity enhancement for the target molecules are approximately 5-fold for the ring resonators and 7-fold for the photonic crystals functionalized by the in situ synthesis method. The larger resonance shifts for the MHD photonic crystal

dx.doi.org/10.1021/ph500075g | *ACS Photonics* 2014, 1, 590−597

structure are likely due to an increased number of ssDNA probes within the ~50 nm sized defect holes where the electric field is strongly localized. Prior work demonstrated that the in situ DNA synthesis process is capable of achieving a high density of ssDNA molecules inside 30−60 nm sized pores in silicon.[31] Hence, the increased number of probe molecules within the photonic crystal defect holes along with the strong light−matter interaction inside the defect holes gives higher detection sensitivity enhancement factors in the MHD photonic crystals. This result highlights the importance of optimizing probe molecule coverage in regions of strong light−matter interaction and shows the potential of the in situ probe synthesis method for achieving improved probe surface coverage on silicon photonic sensors.

To verify the selectivity of the ring resonators and photonic crystal sensors toward the complementary nucleic acid sequence and to rule out the possibility that measured spectral shifts were due to nonspecific binding events, two types of control experiments were performed. Nonspecific binding of ssPNA target molecules was tested by exposing the ssPNA to ring resonators and photonic crystals functionalized only with linker molecules (i.e., no complementary ssDNA probes). In addition, ring resonators and photonic crystals functionalized by the in situ synthesis or conjugation method for ssDNA probe attachment were exposed to noncomplementary ssPNA sequences. For both types of control tests, negligible resonance shifts were observed in all cases. The measured transmission spectra are shown in Figure S3 in the Supporting Information.

Quantification of Probe Molecule Surface Coverage. In order to quantify the ssDNA probe density on the silicon photonic sensor surfaces, ssDNA fluorescently labeled with FAM6 (absorbance peak at 495 nm; emission peak at 520 nm) was utilized for both the in situ synthesis and direct conjugation approaches. The fluorescently labeled ssDNA probes were attached to planar silicon samples for these measurements instead of the silicon photonic structures for ease of examination by a fluorescent microscope (i.e., uniform focal depth and attachment over a large area). As shown in Figure 5a, the fluorescence intensity of the in situ synthesized ssDNA probes is approximately 4 times higher than that of the ssDNA probes immobilized by direct conjugation, as estimated using image processing software (ImageJ). This implies that the surface coverage of in situ synthesized ssDNA probes is at least 4 times higher than directly conjugated ssDNA probes. Note that the sample prepared by direct conjugation of the fluorescently labeled ssDNA probes exhibited multiple bright dots in the fluorescence image attributed to cluster formations, as shown in Supplementarty Information Figure S4-1, which may result from silane aggregation; these ssDNA clusters are likely not fully accessible for hybridization.[32,33] The absolute probe density on the surface cannot be quantified solely from the brightness of fluorescence images since it is difficult to obtain a known standard surface density of the FAM6 fluorescence dye. When known concentrations of FAM6-labeled DNA molecules were drop cast onto silicon wafers, the resulting coffee ring effect (see Supporting Information Figure S4-2) precluded accurate image analysis: ssDNA molecules were not evenly distributed over the silicon surface and exhibited significant aggregation toward the edges of the sample. Therefore, to quantify the surface area coverage of ssDNA probe sequences, measurements were performed in the solution phase. Figure 5b shows the absorbance spectra for FAM6-labeled ssDNA in solution at various concentrations. The resulting calibration curve that links the peak absorbance intensity at 495 nm with FAM6 concentration is presented in Supporting Information Figure S4-3. In order to obtain a solution-phase absorbance measurement of the FAM6-labeled ssDNA probes attached to the silicon sample, the ssDNA must be cleaved from the surface. Accordingly, a slightly different surface chemistry for the directly conjugated ssDNA probes was employed, as described in the Methods section with additional detail provided in the Supporting Information (S5). Experiments were performed to verify that the average resonance shifts due to ssDNA probe and ssPNA target attachment did not change when the cleavable linker was utilized. Hence, the estimated surface density of ssDNA probes estimated by the solution phase measurement is indicative of the surface density of ssDNA probes on the silicon photonic sensors functionalized by the direct conjugation approach for probe molecule attachment. As shown in Figure 5b and Figure S4-3, the concentration of the cleaved ssDNA probes is estimated to be ~130 nM. Note that the presence of the second absorption peak near 343 nm in Figure 5b for the solution containing molecules cleaved from the silicon surface corresponds to the presence of cleavable linker molecules that did not react with ssDNA probes (see Supporting Information S5 for details) and confirms that the directly conjugated ssDNA probe molecules attach to only a fraction of the available linker sites on the sample surface. Since the surface area of the silicon sample onto which the ssDNA probes were attached was approximately 3.6 cm^2 and the total volume of solution used for the measurement was 250 μL, the overall surface density of the directly conjugated ssDNA probes is estimated to be 5×10^{12} /cm^2. This surface density is consistent with other reports of DNA surface densities on planar surfaces.[34−36] On the basis of the intensity comparison of fluorescence images in Figure 5a and the resonance shift data presented in Figure 3 and Figure 4, the ssDNA probe surface density on silicon photonic structures functionalized by the in situ synthesis method is estimated to be at least 2×10^{13} /cm^2.

Faster Response Time with Increased Probe Molecule Surface Coverage. By integrating PDMS microchannels with the silicon photonic sensors (see Supporting Information S6 for more details), the measured transmission spectra can be monitored in real-time to ascertain the influence of probe molecule surface density on the binding kinetics of target molecules. A 1 μM complementary ssPNA solution was injected at a constant flow rate of 0.003 mL/min into the flow cells. The time-dependent resonance shifts of silicon ring resonators functionalized with either in situ synthesized ssDNA probe molecules or directly conjugated ssDNA probe molecules are shown in Figure 6. Following ssPNA hybridization, nonspecifically bound ssPNA molecules were rinsed away by flowing DI water through the microchannels; small blue shifts can be observed in Figure 6 for both ring resonator samples following the rinsing. The kinetic binding rates for ssPNA target sequences onto the silicon photonic sensors were obtained by a simple linear fit to the two time-dependent resonance shift curves in the presaturation regime (first 40 min). For the case of the ring resonator functionalized with in situ synthesized ssDNA probes, $\Delta\lambda/\Delta t$ = 9.6 pm/min, while for the ring resonator functionalized with conjugated ssDNA probe molecules $\Delta\lambda/\Delta t$ = 2.7 pm/min. Accordingly, the kinetic binding rate and response time of silicon photonic biosensors are approximately 3.5 times faster when the sensor is functionalized using the in situ synthesis method for probe

dx.doi.org/10.1021/ph500075g | ACS Photonics 2014, 1, 590−597

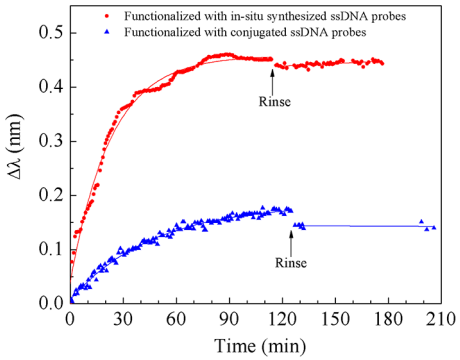

Figure 6. Kinetic binding curves for ssPNA target sequences using microfluidic channels as an analyte delivery system to 5 μm radius silicon ring resonators functionalized with either in situ synthesized or directly conjugated ssDNA probe molecules. The solid lines connecting data points taken before the rinse step indicate exponential fits of the kinetic binding rates of ssPNA for the two different rings. The faster response time of the ring functionalized with in situ synthesized probes is proportional to the increased probe surface coverage on that ring.

molecule functionalization, which allows for higher probe molecule coverage than direct conjugation approaches. Faster binding rates can likely be achieved by increasing the flow rate.[7] Note that in this flow cell experiment the resonance shift for ssPNA target hybridization on a silicon ring resonator functionalized with in situ synthesized ssDNA probe sequences is smaller than the average resonance shift reported in Figure 3. This smaller resonance shift is attributed to a loss of ssDNA probe molecules that likely occurs during attachment and curing of the PDMS microfluidic channel. In future experiments, it may be possible to modify the DNA synthesizer tool to accommodate attachment of in situ synthesized ssDNA probe molecules delivered through a flow cell. For the ring resonator functionalized by directly conjugated ssDNA probes, all surface functionalization steps were carried out by microfluidics delivery within the PDMS flow cell, and the resulting ssPNA target resonance shift is comparable to the average resonance shift reported in Figure 3. By examining the resonance shifts upon ssPNA target molecule binding for the two different functionalized ring resonators in Figure 6 (~3.2:1 for in situ synthesized:directly conjugated ssDNA probes functionalization) and assuming the probe surface coverage ratio is similar to the ssPNA resonance shift ratio, it can be concluded that the kinetic binding rate scales approximately with the bioreceptor surface area coverage. Complete integration of microfluidics with silicon photonic sensors functionalized with in situ synthesized ssDNA probes could enable individual array elements on multiple sensors to be functionalized with the same probe sequences at the same time. This would facilitate the functionalization of multiple array sensors with different sequences in the same amount of time required to functionalize a single array sensor with multiple sequences.

CONCLUSION

We demonstrate the importance of achieving high probe molecule surface area coverage over the active sensing regions of silicon photonic devices that are progressively utilizing smaller footprints and realizing increased modal confinement over subwavelength dimensions. An in situ ssDNA probe synthesis technique was utilized to increase the surface coverage of ssDNA probe molecules by 5−7 times on silicon microring resonators and photonic crystals compared to standard probe molecule conjugation techniques. The enhanced probe surface coverage led to a 5−7 times enhancement in the measured resonance wavelength shifts upon target molecule capture, suggesting that the probe molecule density is below that which would cause steric hindrance of hybridization events. Fluorescence measurements quantified the density of the in situ synthesized ssDNA probes to be on the order of $10^{13}/cm^2$. The enhanced probe molecule coverage achieved by using the in situ synthesis technique also led to a more than 3-fold reduction in the response time of the silicon photonic sensors. These results suggest improved detection sensitivities and response times for sub-nanomolar target biomolecule concentrations are achievable. Integration of the label-free, functionalized photonic devices with microfluidics and high-throughput multiplexing via cascaded devices has exciting possibilities for point-of-care, lab-on-a-chip sensor development.

METHODS

Device Fabrication. The microring resonators and photonic crystals are fabricated on silicon-on-insulator (SOI) wafers with a 3 μm thick buried oxide layer (SOITEC). The thickness of the silicon device layer is 270 nm for the ring resonators and 220 nm for the photonic crystals. The wafers were cleaved and coated with a 300 nm ZEP520A photoresist (6000 rpm for 45 s). Electron beam lithography was performed using a JEOL9300FS tool at 100 kV voltage, 400 $\mu C/cm^2$. Following exposure, the samples were developed in xylenes for 30 s and rinsed thoroughly with isopropyl alcohol (IPA). The photoresist pattern was then transferred into the silicon layer by reactive ion etching (Oxford PlasmaLab 100) using C_4F_8/SF_6/Ar gases to completely etch the exposed portion of the silicon layer. To further increase the index contrast for the photonic crystals, an undercut was performed to introduce an air gap between the device layer and the substrate. For the undercut procedure, the sample was cleaned with IPA and then baked on a hot plate at 115 °C for 10 min to fully remove absorbed water and IPA on the surface. AZ1513 photoresist was spin coated onto the sample at 4000 rpm for 45 s. Next, the sample was soft baked on a hot plate at 95 °C for 50 s and then exposed under a mask aligner at 70 mJ/cm^2 (Karl Suss MA6). An AZ MIF developer was used for 1 min, and the sample was then placed on a hot plate for 10 min at 115 °C to facilitate photoresist cross-linking. Finally, the sample was soaked in buffered oxide etchant (10:1) for 20 min to etch ~1 μm of the buried oxide layer. The sample was rinsed with DI water and dried under nitrogen before measurements.

Transmission Measurements. Near-infrared light from a tunable continuous wave laser (1500 to 1630 nm, Santec TSL-510) was coupled into and out from millimeter-length bus waveguides using polarization-maintaining lensed fibers (OZ Optics Ltd.) mounted on piezo-controlled XYZ stages. Photodetection of the transmitted light was performed using a fiber-coupled avalanche photodiode photoreceiver (Newport 1647).

Surface Functionalization. To perform biosensing, the sample surface was first passivated by thermal oxidation. Samples were rinsed with DI water, acetone, and IPA three times each and then cleaned with piranha solution for 10 min at 120 °C. The samples were then oxidized in an oven in an ambient air environment at 500 °C for 10 min.

dx.doi.org/10.1021/ph500075g | ACS Photonics 2014, 1, 590−597

Probe DNA Attachment Using in Situ Synthesis Method. Before DNA attachment, the sample surface needs to be functionalized with hydroxyl groups for the in situ synthesis technique. Accordingly, samples were silanized with 4% *N*-(3-triethoxysilylpropyl)-4-hydroxybutyramide (TEOS-HBA) in ethanol and deionized (DI) water for 4 h and then rinsed thoroughly with DI water and dried under nitrogen. The samples were then annealed in an oven at 200 °C for 16 h. In order to form stable, cross-linked silane films, hydrolysis was performed after annealing: samples were soaked in DI water for 4 h to remove any unreacted silane molecules. Each sample was then placed in a custom-designed sample holder in an Applied Biosystems model 392 DNA synthesizer for base-by-base attachment of the 16-mer probe DNA using the phosphoramidite method. By this method, each DNA base that is added is charge neutral owing to an attached protecting group and is much smaller than the full ssDNA sequence.[31] Steric hindrance is therefore greatly mitigated in the case of in situ synthesized ssDNA compared to the direct conjugation method. After synthesis, DNA molecules were deprotected in 1:1 ethylenediamine/ethanol solution for 30 min to activate them for future hybridization.[37] The samples were then soaked in ethanol for 30 min, rinsed with ethanol, and dried under nitrogen. For the samples used in fluorescence imaging, DNA probe sequences were labeled with FAM-6 fluorescence dye at the 5′ end. The FAM-6 fluorescence dye was deprotected using the same 1:1 ethylenediamine/ethanol solution for 30 min.

Probe DNA Attachment Using Direct Conjugation Method. The samples were soaked in a 1% 3-aminopropyltriethoxysilane (3-APTES) solution in anhydrous toluene for 15 min and then rinsed with toluene and ethanol three times to remove excess unreacted 3-APTES molecules. The samples were annealed in an oven in air ambient at 150 °C for 20 min to promote cross-linking among the silane molecules and increased stability in aqueous media. After silanization, the samples were incubated in 2.5 mg/mL sulfosuccinimidyl-4-(*N*-maleimidomethyl)cyclohexane-1-carboxylate (Sulfo-SMCC, Pierce) in 4-(2-hydroxyethyl)-1-piperazineethanesulfonic acid (HEPES) buffer for 2 h, rinsed with HEPES buffer, and soaked in HEPES buffer for another 1 h to ensure all unreacted silane molecules were removed. An excess (100 μM) of 16-mer thiol modified probe DNA (5′-TAG CTA TGG TCC TCG T-3′, 3′ Thiol C3, Eurofins MWG Operon) in HEPES buffer was mixed 1:1 by volume with disulfide reducing agent tris(2-carboxyethyl)phosphine (TCEP, Pierce) in DI water and ethanol for 30 min and then pipetted onto the sample. After 1 h incubation at 37 °C, the sample was soaked in HEPES buffer for 20 min at 37 °C, rinsed with DI water, and dried with nitrogen gas to remove any remaining unattached molecules. For the fluorescence measurements performed to quantify probe molecule surface coverage, the probe DNA was purchased with a FAM-6 fluorescent label, and a cleavable linker molecule, *N*-succinimidyl-3-(2-pyridyldithio)propionate (SPDP), was substituted for Sulfo-SMCC. After the silanization process described above, the sample was incubated in 6.5 mM SPDP in ethanol for 30 min, then soaked in IPA for 10 min and rinsed with IPA and DI water three times each. A 200 μL amount of a 100 μM solution containing thiol-modified FAM6-labeled DNA probes in HEPES buffer was reduced using a beaded resin on which TCEP was immobilized. It is essential that no TCEP is present in the DNA solution; if any TCEP were present in the DNA solution upon exposure to the SPDP-functionalized silicon sample, it would cleave the SPDP from surface before allowing DNA binding. The SPDP-functionalized sample was incubated in the reduced FAM6-labeled DNA probe solution for 1 h, followed by a 20 min soak in HEPES buffer. Next, the DNA was cleaved from the surface through exposure to 250 μL of 2 mM TCEP in HEPES buffer for 30 min. Since the FAM6 florescence dye is sensitive to pH (an acid environment will oxidize the dye and quench florescence), the pH of the TCEP solution was adjusted to around 7.5 using sodium hydroxide. Finally, the TCEP solution was collected into a quartz cuvette for quantification of the probe molecule concentration by absorbance measurements.

Target PNA Attachment. Complementary PNA sequences (ACG AGG ACC ATA GCT A, BioSynthesis) were chosen as the target molecules. Complementary PNA in DI water at a concentration of either 1 or 100 μM was pipetted onto each sample and incubated at 37 °C for 1 h. Samples were then soaked in HEPES buffer for 20 min to remove unhybridized oligos, thoroughly rinsed with DI water, and dried under nitrogen.

Fluorescence and Absorbance Measurements. Florescence images were taken using a Nikon AZ100 M upright florescence microscope. Absorbance spectra of fluorescently tagged DNA in solution were collected over a wavelength range of 300 to 550 nm in a Varian Cary 5000 UV−vis−NIR spectrophotometer at a step size of 0.5 nm.

■ ASSOCIATED CONTENT

Supporting Information

Supporting Information is available free of charge via the Internet at http://pubs.acs.org.

■ AUTHOR INFORMATION

Corresponding Author

*E-mail: sharon.weiss@vanderbilt.edu.

Notes

The authors declare no competing financial interest.

■ ACKNOWLEDGMENTS

This work was funded in part by the National Science Foundation (EECS0925642 and ECCS0746296). A portion of this research was conducted at the Center for Nanophase Materials Sciences, which is sponsored at Oak Ridge National Laboratory by the Scientific User Facilities Division, Office of Basic Energy Sciences, U.S. Department of Energy. Equipment and technical support in the Vanderbilt Institute for Nanoscale Science and Engineering and Vanderbilt Institute for Integrative Biosystems Research and Education were also utilized for this work. The authors gratefully acknowledge D. P. Briggs for assistance with sample fabrication, K. R. Beavers for assistance with chemistry, J. D. Ryckman and Y. Jiao for assistance with sample fabrication and optical characterization, and P. E. Laibinis, G. Gaur, X. Wei, and C. Kang for useful technical discussions.

■ REFERENCES

(1) Gervais, L.; de Rooij, N.; Delamarche, E. Microfluidic Chips for point-of-care immunodiagnostics. *Adv. Mater.* **2011**, *23*, H151−H176.
(2) Lequin, R. M. Enzyme immunoassay (EIA)/enzyme-linked immunosorbent assay (ELISA). *Clin. Chem.* **2005**, *51*, 2415−2418.
(3) Settle, M.; Salib, M.; Michaeli, A.; Krauss, T. F. Low loss silicon on insulator photonic crystal waveguides made by 193nm optical lithography. *Opt. Express* **2006**, *14*, 2440−2445.

(4) Quan, F. L.; Nigel, C.; Parth, P.; Marko, L. Qimin, scalable photonic crystal chips for high sensitivity protein detection. *Opt. Express* **2013**, *21*, 32306−32312.
(5) Iqbal, M.; Gleeson, M. A.; Spaugh, B.; Tybor, F.; Gunn, W. G.; Hochberg, M.; Baehr-Jones, T.; Bailey, R. C.; Gunn, L. C. Label-free biosensor arrays based on silicon ring resonators and high-speed optical scanning instrumentation. *IEEE J. Sel. Top. Quantum Electron.* **2010**, *16*, 654−661.
(6) Qavi, A. J.; Kindt, J. T.; Gleeson, M. A.; Bailey, R. C. Anti-DNA:RNA antibodies and silicon photonic microring resonators: increased sensitivity for multiplexed microRNA detection. *Anal. Chem.* **2011**, *83*, 5949−5956.
(7) Qavi, A. J.; Mysz, T. M.; Bailey, R. C. Isothermal discrimination of single-nucleotide polymorphisms via real-time kinetic desorption and label-free detection of DNA using silicon photonic microring resonator arrays. *Anal. Chem.* **2011**, *83*, 6827−6833.
(8) Niehusmann, J.; Vorckel, A.; Bolivar, P. H.; Wahlbrink, T.; Henschel, W.; Kurz, H. Ultrahigh-quality-factor silicon-on-insulator microring resonator. *Opt. Lett.* **2004**, *29*, 2861−2863.
(9) Xia, F. N.; Sekaric, L.; Vlasov, Y. Ultracompact optical buffers on a silicon chip. *Nat. Photonics* **2007**, *1*, 65−71.
(10) Xu, Q.; Fattal, D.; Beausoleil, R. G. Silicon microring resonators with 1.5 μm radius. *Opt. Express* **2008**, *16*, 4309−4315.
(11) Akahane, Y.; Asano, T.; Song, B. S.; Noda, S. High-Q photonic nanocavity in a two-dimensional photonic crystal. *Nature* **2003**, *425*, 944−947.
(12) Quan, Q. M.; Deotare, P. B.; Loncar, M. Photonic crystal nanobeam cavity strongly coupled to the feeding waveguide. *Appl. Phys. Lett.* **2010**, *96*, 203102.
(13) Song, B. S.; Noda, S.; Asano, T.; Akahane, Y. Ultra-high-Q photonic double-heterostructure nanocavity. *Nat. Mater.* **2005**, *4*, 207−210.
(14) Altug, H.; Englund, D.; Vuckovic, J. Ultrafast photonic crystal nanocavity laser. *Nat. Phys.* **2006**, *2*, 484−488.
(15) Reed, G. T.; Mashanovich, G.; Gardes, F. Y.; Thomson, D. J. Silicon optical modulators. *Nat. Photonics* **2010**, *4*, 518−526.
(16) Matsuo, S.; Shinya, A.; Kakitsuka, T.; Nozaki, K.; Segawa, T.; Sato, T.; Kawaguchi, Y.; Notomi, M. High-speed ultracompact buried heterostructure photonic-crystal laser with 13 fJ of energy consumed per bit transmitted. *Nat. Photonics* **2010**, *4*, 648−654.
(17) Lee, M.; Fauchet, P. M. Two-dimensional silicon photonic crystal based biosensing platform for protein detection. *Opt. Express* **2007**, *15*, 4530−4535.
(18) Xu, D. X.; Vachon, M.; Densmore, A.; Ma, R.; Delage, A.; Janz, S.; Lapointe, J.; Li, Y.; Lopinski, G.; Zhang, D.; Liu, Q. Y.; Cheben, P.; Schmid, J. H. Label-free biosensor array based on silicon-on-insulator ring resonators addressed using a WDM approach. *Opt. Lett.* **2010**, *35*, 2771−2773.
(19) McClellan, M. S.; Domier, L. L.; Bailey, R. C. Label-free virus detection using silicon photonic microring resonators. *Biosens. Bioelectron.* **2012**, *31*, 388−392.
(20) Byeon, J. Y.; Bailey, R. C. Multiplexed evaluation of capture agent binding kinetics using arrays of silicon photonic microring resonators. *Analyst* **2011**, *136*, 3430−3433.
(21) Kang, C.; Weiss, S. M. Photonic crystal with multiple-hole defect for sensor applications. *Opt. Express* **2008**, *16*, 18188−18193.
(22) Kang, C.; Phare, C. T.; Vlasov, Y. A.; Assefa, S.; Weiss, S. M. Photonic crystal slab sensor with enhanced surface area. *Opt. Express* **2010**, *18*, 27930−27937.
(23) Pal, S.; Guillermain, E.; Sriram, R.; Miller, B. L.; Fauchet, P. M. Silicon photonic crystal nanocavity-coupled waveguides for error-corrected optical biosensing. *Biosens. Bioelectron.* **2011**, *26*, 4024−4031.
(24) Chakravarty, S.; Zou, Y.; Lai, W. C.; Chen, R. T. Slow light engineering for high Q high sensitivity photonic crystal microcavity biosensors in silicon. *Biosens. Bioelectron.* **2012**, *38*, 170−176.
(25) Kang, C.; Weiss, S. M.; Vlasov, Y. A.; Assefa, S. Optimized light-matter interaction and defect hole placement in photonic crystal cavity sensors. *Opt. Lett.* **2012**, *37*, 2850−2852.
(26) Chakravarty, S.; Lai, W. C.; Zou, Y.; Drabkin, H. A.; Gemmill, R. M.; Simon, G. R.; Chin, S. H.; Chen, R. T. Multiplexed specific label-free detection of NCI-H358 lung cancer cell line lysates with silicon based photonic crystal microcavity biosensors. *Biosens. Bioelectron* **2013**, *43*, 50−55.
(27) Huizenga, D. E.; Szostak, J. W. A DNA aptamer that binds adenosine and ATP. *Biochemistry* **1995**, *34*, 656−665.
(28) Du, Y.; Li, B. L.; Wei, H.; Wang, Y. L.; Wang, E. K. Multifunctional label-free electrochemical biosensor based on an integrated aptamer. *Anal. Chem.* **2008**, *80*, 5110−5117.
(29) Bogaerts, W.; De Heyn, P.; Van Vaerenbergh, T.; De Vos, K.; Selvaraja, S. K.; Claes, T.; Dumon, P.; Bienstman, P.; Van Thourhout, D.; Baets, R. Silicon microring resonators. *Laser Photonics Rev.* **2012**, *6*, 47−73.
(30) Kang, C.; Weiss, S. M.; Vlasov, Y. A.; Assefa, S. Optimized light-matter interaction and defect hole placement in photonic crystal cavity sensors. *Opt. Lett.* **2012**, *37*, 2850−2852.
(31) Lawrie, J. L.; Jiao, Y.; Weiss, S. M. Size-dependent infiltration and optical detection of nucleic acids in nanoscale pores. *IEEE Trans. Nanotechnol.* **2010**, *9*, 596−602.
(32) Vandenberg, E. T.; Bertilsson, L.; Liedberg, B.; Uvdal, K.; Erlandsson, R.; Elwing, H.; Lundstrom, I. Structure of 3-aminopropyl triethoxy silane on silicon-oxide. *J. Colloid Interface Sci.* **1991**, *147*, 103−118.
(33) Aissaoui, N.; Bergaoui, L.; Landoulsi, J.; Lambert, J. F.; Boujday, S. Silane layers on silicon surfaces: mechanism of interaction, stability, and influence on protein adsorption. *Langmuir* **2012**, *28*, 656−665.
(34) Steel, A. B.; Levicky, R. L.; Herne, T. M.; Tarlov, M. J. Immobilization of nucleic acids at solid surfaces: effect of oligonucleotide length on layer assembly. *Biophys. J.* **2000**, *79*, 975−981.
(35) Lee, C. Y.; Gong, P.; Harbers, G. M.; Grainger, D. W.; Castner, D. G.; Gamble, L. J. Surface coverage and structure of mixed DNA/alkylthiol monolayers on gold: characterization by XPS, NEXAFS, and fluorescence intensity measurements. *Anal. Chem.* **2006**, *78*, 3316−3325.
(36) Peterson, A. W.; Heaton, R. J.; Georgiadis, R. M. The effect of surface probe density on DNA hybridization. *Nucleic Acids Res.* **2001**, *29*, 5163−5168.
(37) Lawrie, J. L.; Xu, Z.; Rong, G. G.; Laibinis, P. E.; Weiss, S. M. Synthesis of DNA oligonucleotides in mesoporous silicon. *Phys. Status Solidi A* **2009**, *206*, 1339−1342.